

A time-to-digital converter with steady calibration through single-photon detection

Matías R. Bolaños Wagner,¹ Daniele Vogrig,¹ Paolo Villorosi,^{1,2,3} Giuseppe Vallone,^{1,2,3} and Andrea Stanco^{1,2,3,*}

¹*Dipartimento di Ingegneria dell'Informazione, Università degli Studi di Padova, Via Gradenigo 6B - 35131 Padova, Italy.*

²*Padua Quantum Technologies Research Center, Università degli Studi di Padova, via Gradenigo 6B, IT-35131 Padova, Italy*

³*Istituto Nazionale di Fisica Nucleare (INFN) – sezione di Padova, Italy*

(Dated: June 4, 2024)

Time-to-Digital Converters (TDCs) are a crucial tool in a wide array of fields, in particular for quantum communication, where time taggers performance can severely affect the quality of the entire application. Nowadays, FPGA-based TDCs present a viable alternative to ASIC ones, once the nonlinear behaviour due to the intrinsic nature of the device is properly mitigated. To compensate said nonlinearities, a calibration procedure is required, usually based on an interpolation methods. Here we present the design and the demonstration of a TDC that is FPGA-based and showing a residual jitter of 27 ps, that is scalable for multichannel operation. The application in Quantum Key Distribution (QKD) is discussed with a unique calibration method based on the exploitation of single-photon detection that does not require to stop the data acquisition or to use any interpolation methods, thus increasing accuracy and removing data loss. The calibration was tested in a relevant environment, investigating the device behaviour between 5°C and 80°C. Moreover, our design is capable of continuously streaming up to 12 Mevents/s for up to ~ 1 week without the TDC overflowing.

I. INTRODUCTION

Time-to-digital converters (TDCs) are used in a wide range of applications [1, 2] where picosecond resolution is needed for time detection, such as high-energy particle physics [3], light detection and ranging (LiDAR) [4], quantum communications [5–7] and quantum random number generation [8]. Recently, Field-Programmable Gate Arrays (FPGAs) have emerged as a popular platform for implementing TDCs due to their flexibility, high-speed performance, and cost-effectiveness [9–12]. However, standard FPGA-based TDCs require periodic calibration to maintain accuracy, which requires either interpolation methods or stopping the data acquisition process, leading to potential data loss and reduced efficiency [13]. Although it is possible to optimize and automatize the calibration procedure [14–16], to the best of our knowledge, there are no proposals to overcome the data losses.

Quantum Key Distribution (QKD) allow two parties (Alice and Bob) to create a shared, secret key. To do so, Alice encodes the information in degrees of freedom of a given quantum system, usually photons [17]. To make the sharing of the key successful, Bob requires precise timing of arrival of photons to synchronize both parties effectively, and to allow better distinguishability between signal and noise. For example, algorithms like Qubit4Sync allow Bob to reconstruct Alice’s clock signal from his own qubit measurements [18]. Moreover, QKD is currently evolving to be implemented using satellite links to increase the distance achievable with this protocols [19]. This implies that communication could only be done while the satellite passes through the ground station’s field of view. During this limited time, Bob should

receive as much data as possible while maintaining its performance, implying that both calibrating or losing calibration mid-measurement can considerably hinder key generation.

In this work, we propose an FPGA-based TDC, named *MARTY* and implemented on a Zynq7020, that addresses the calibration challenge by integrating a so-called *steady calibration*¹ method, implemented by exploiting single-photon detection, similarly to what is done in [20] but in a different application framework. This method allows the TDC to calibrate itself using the data it acquires, eliminating the need to stop the acquisition process. This feature not only enhances the efficiency of the system, but also improves the overall time accuracy as each measurement is also a contribution to calibration and there is no distinction between “data-acquisition” and “calibration” phases.

The paper has the following structure: in Section II we present the working principle of the system, including the FPGA design, normal and steady calibration procedures, and finally how we performed temperature variation tests on the device; in section III we present the results obtained in this work, including a QKD test performed with *MARTY*; eventually, in section IV we present the final conclusions and future perspectives.

¹ We chose the term “steady calibration” as the terms “self-calibration”, “automatic calibration” or “real-time calibration” are standard forms to indicate just an online calibration procedure which usually include a phase of data loss.

* andrea.stanco@unipd.it

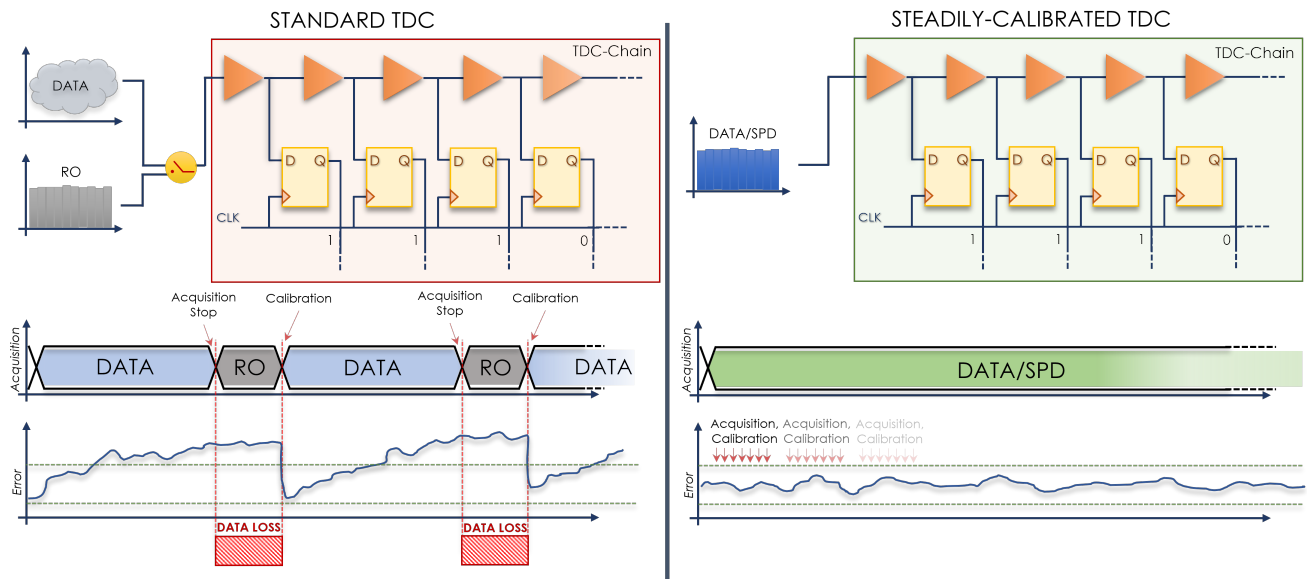


FIG. 1: Functioning principle of a steadily-calibrated TDC (right) compared with a normal TDC (left).

II. MATERIALS AND METHODS

A. Design of the device

A generic TDC channel can consist of two components: a clock counting module for the coarse time estimation and a tapped delay line (TDL) for the fine estimation (Fig. 1 left).

While the clock counting module is a binary counter that increases at each rising edge of a clock, the TDL is a “propagation line” where the electric signal travels through a chain of similar elements, each one with an intrinsic propagation delay. The implementation of such structure can be realized in different ways. In MARTY, for the coarse counting module, the DSP48 components were used as they grant high efficiency and speed, clocked by a $f_s = 412.5$ MHz clock, Φ_{sample} . With the given clock frequency and the choice of encoding the coarse counter in 48 bits, MARTY has a total runtime of $2^{48}/f_s \sim 1$ week before overflow.

The TDL was implemented through a chain of fast-carry components, the CARRY4 element (each containing 4 fast-carry). As usual in TDC implementation, each point of the TDL is flip-flopped in order to snapshot the current state at each clock edge. This snapshot output can be considered as a thermometer code that characterizes the propagation time inside the TDL and can be translated into a binary code using a dedicated decoder. The decoding algorithm used in MARTY was the one presented by *Adamič et al.* in [21], which is based on a pipelined adder tree. This algorithm was chosen due to its high robustness against ‘bubble errors’ without increasing the complexity of the system. ‘Bubbles’ behave like a ‘bit swap’ between two neighbouring bits of the thermometer code (e.g. a code that should be 11111000

instead appears as 11110100), and they appear due to a variety of effects such as metastability on the flip-flops used to snapshot the TDL state [1].

It is worth to notice that the propagation time inside each fast-carry component is not uniform, ranging from units of picoseconds to around 100 ps. Therefore, a calibration is needed to precisely characterize such propagation times. By using 36 CARRY4 elements (144 fast-carry components in total), the coarse period $\tau_{\text{coarse}} = 1/f_s \simeq 2.42$ ns was fully covered. Indeed, a maximum length of $N_c \in [130, 136]$ bins was obtained in all data acquisitions.

The final timestamp is obtained by combining the binary value of the TDL thermometer code, named *fine value*, and the value obtained from the clock counting module, named *coarse value*. The output timestamps of a channel can then be stored in a block RAM (BRAM) module to later transfer them to an external PC.

The device takes advantage of the System-on-a-Chip (SoC) technology, exploiting not only the FPGA but also the CPU(s) counterpart to implement a real-time data transfer from the BRAM to the PC via Ethernet protocol [22]. This scheme allows to continuously stream the TDC data from the FPGA to the PC with the only limitation of the Ethernet capability, bringing to an acquisition speed of up to 15 Mevents/s without data loss. Furthermore, to facilitate software integration, a request-based scheme was also implemented, as it is a standard approach on commercial TDCs to transfer data to a PC. In this scheme, the acquired data is sent only when receiving an external request from a PC.

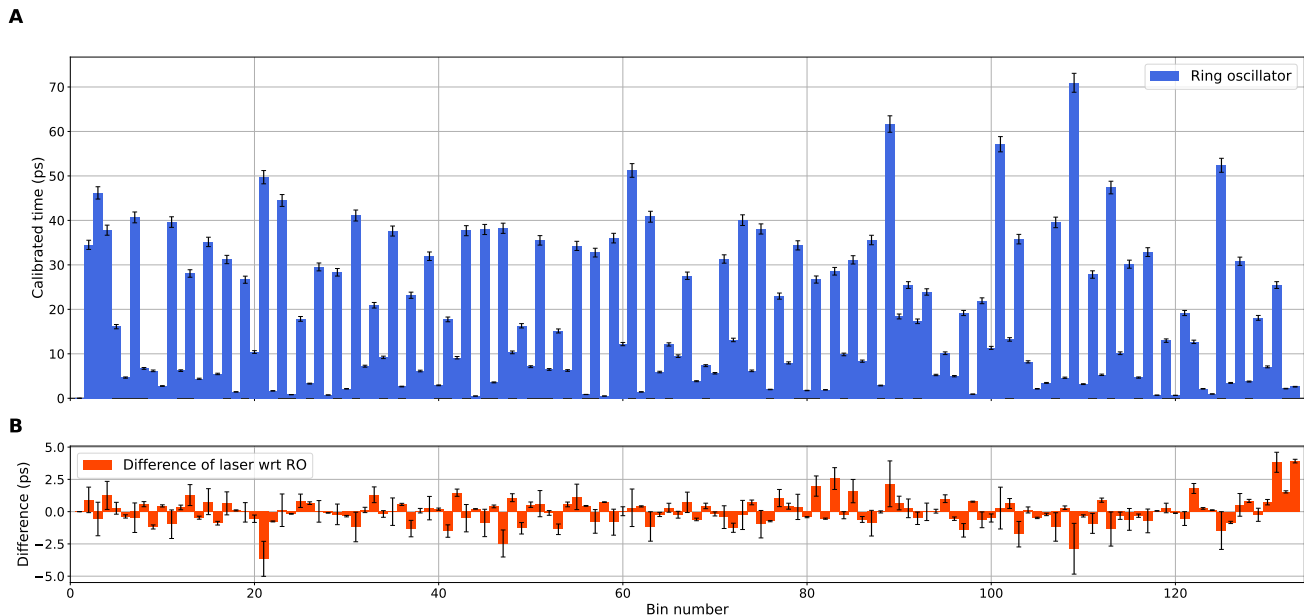


FIG. 2: (a) Histogram obtained with a code density test using an FPGA-based RO as input. (b) Percentile difference of the histogram obtained with a code density test using a laser detection signal with respect to the RO one.

B. System calibration and auto-calibration

The calibration method is based on the evaluation of the results of a *code density* test. A code density test consists of using a signal uniformly distributed over the time spanned by the TDL ($1/f_s \approx 2.42$ ns), and measuring the number of occurrences obtained from each bin. If the input signal is uniformly distributed and enough events were recorded, the occurrences in each bin should be proportional to its propagation time [2]. As a standard solution, the code density test is performed using an internal Ring Oscillator (RO)², that generates a uniformly-distributed signal connected to the input of the TDC. To obtain the minimum number of events needed to calibrate, N_{events} , the method proposed in [23] was used, such that

$$N_{events} > \left(\frac{z_{\alpha/2}}{\beta} \right)^2 \cdot (M - 1), \quad (1)$$

where $z_{\alpha/2}$ corresponds to the area under the standard normal distribution curve of $\alpha/2$, $M = 8$ the number of bits, $\beta = 0.02$ represents a tolerance of 2% and $\alpha = 0.01$ represents a confidence interval of 99%, from which the required number of events $N_{events} > 116110$ was obtained.

From the number of events detected in the bin i , w_i , it is possible to derive the propagation time of the calibrated bin $\delta t_i = \frac{w_i}{\sum_j w_j} \tau_{sample}$, with $i \in [1, N_c]$ (Fig. 2).

Then, the calibrated time is defined as

$$t_i^{(c)} = \frac{1}{2} \delta t_i + \sum_{j < i} \delta t_j. \quad (2)$$

This type of calibration requires the user to stop the current acquisition for around 30 ms, switching from the input signal to the RO one.

In this work, we propose an extension of this method, called *steady calibration*, which allows the system to continuously calibrate while the device is acquiring data (Fig. 1 right). This method consists of storing the code density histogram in an ordered manner, so that at each new detected event, the first one of the histogram is deleted and the new one is appended at the end. Then, the calibration curve is recalculated with the new data.

The steady calibration method allows the exploitation of the acquired TDC data to calibrate itself in real time, assuming that the detected events are uniformly distributed over the TDL. Considering a pulsed laser as an event source with the repetition rate f_q disciplined by a clock Φ_{qubit} , the temporal distribution is expected not to be uniform in the TDL outputs only if the two clocks Φ_{qubit} and Φ_{sample} are commensurable, or locked to each other, and perfectly stable without any drift or jitter. Therefore, the combination of non commensurable clock frequencies and drift effects, can assure a uniform distribution of the input events.

To test the proposed method, we obtained the calibration curve using a laser source and a single photon detector (SPD) in place of the integrated RO. When comparing both histograms obtained with a code density test (Fig. 2), the difference between both is considered negligible, with a $\chi^2 = 0.026$. From this, we can conclude

² A ring oscillator consists of an unstable loop of delay elements (usually not-gate) that generates a random output.

that using an external single photon detector with a laser signal is equivalent to the integrated RO in the FPGA chip for calibration purposes.

C. Temperature test setup

The validity of the steady calibration method was verified by forcing a change in the working point of the system, which should require a calibration. Therefore, the device was tested at different temperatures as this can have a relevant impact on the performance of a TDC and is considered strictly related to the TDC calibration process [24]. To modify the device temperature, we used a combination of a Peltier cell and an RAL 9006 climatic chamber by Angelatoni Test Technologies. The combination of both temperature control systems allowed the FPGA chip to reach a broader temperature range, from 5 °C to 80 °C. To measure the temperature of the chip, the included XADC sensor of the board was used, which gives a temperature measurement in the center of the chip itself.

The jitter and resolution of a two-channel implementation of MARTY was used to characterize its performance. To calculate the jitter, an input signal is divided into the two channels, which we assume equal for this purpose, and the histogram of the differences between the timetags is obtained, from which the jitter can be obtained. For this approximation, we assume that both channels have the same jitter and that the jitter of the source does not affect the resulting histogram due to both channels receiving the same input signal.

To perform the temperature measurements, a 1550 nm attenuated laser source was used as an input to a single-photon detector (PMD-IR detector by MPD), which was then divided and used as input for both channels of the TDC. The chip temperature was scanned in the whole range of 5 °C to 80 °C with a step of 1 °C, where for each temperature the jitter and resolution were evaluated.

D. Quantum Key Distribution test setup

To evaluate the device performance for QKD applications, while also comparing it with commercial TDCs, a QKD transmitter like the one proposed in [25] was used to encode an “HVDD” sequence.³ We used a standard polarization receiver scheme with four PMD-IR detectors by MPD, where for the time-tagger we used both a QuTAG from QuTools and MARTY. To evaluate the performance, a detection peak was measured with both devices, and the Quantum Bit Error Rate (QBER) for the HVDD sequence was estimated.

³ An “HVDD” sequence is a sequence of four qubits encoded using single-photon with Horizontal-Vertical-Diagonal-Diagonal polarizations.

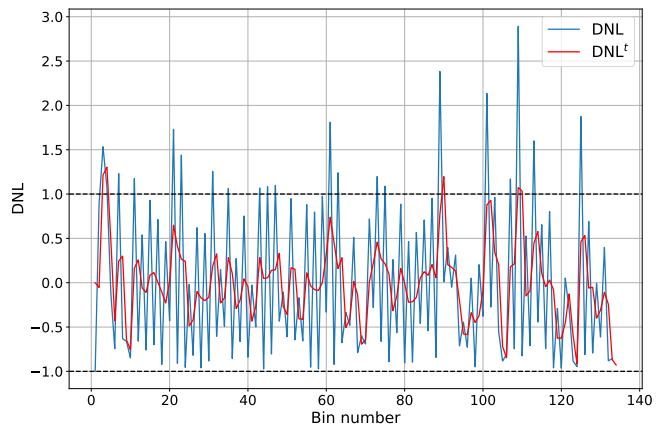


FIG. 3: DNL (in blue) and DNL^t (in red) obtained for a single channel of the TDC at room temperature.

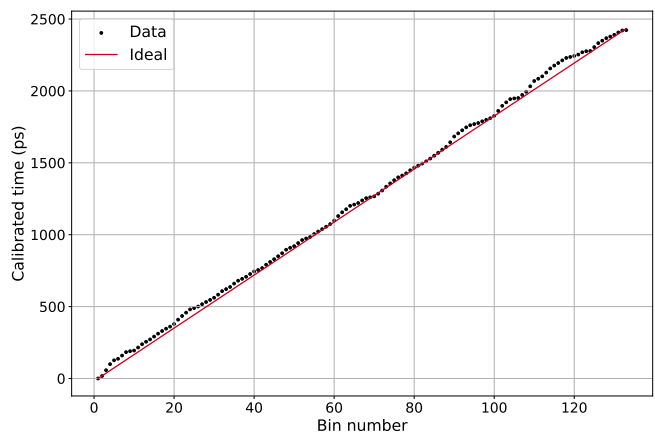


FIG. 4: Calibrated time as a function of the bin number of the TDC, in orange the ideal behaviour for a uniform delay line.

III. RESULTS AND DISCUSSIONS

MARTY’s main performance metrics, such as resolution, differential nonlinearity (DNL), and jitter were characterized using a two-channel TDC configuration. The DNL represents the deviation of the delay line with respect to an ideal one (uniformly distributed in time) and it was evaluated through a code density test with an internal RO as the input of the TDC, obtaining the counts for bin i , w_i (Fig. 2a), from which the DNL was obtained as

$$DNL_i = \frac{w_i - \langle w \rangle}{\langle w \rangle}, \quad (3)$$

where $\langle w \rangle = \sum_{i=1}^{N_c} \frac{w_i}{N_c}$, and N_c is the last bin for which counts were recorded (Fig. 3). A $DNL = [-0.97, 2.86]$ was obtained, but at room temperature only 21 out of the 133 bins had $DNL > 1$. Once the linearity was characterized, the mean resolution of the system was evaluated.

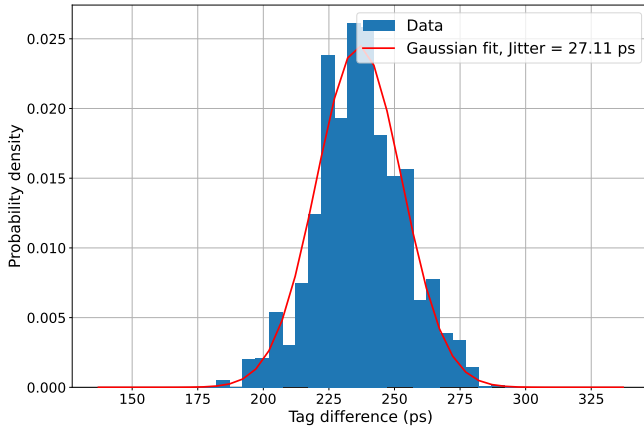


FIG. 5: Histogram of the difference between two consecutive timetags in a two-channel implementation. In red, the corresponding Gaussian fit, from which the jitter was estimated.

To do so, after obtaining the calibrated time curve $t_i^{(c)}$ (Fig. 4), the last element of the curve was divided by the total amount of active bins N_c , so a resolution of

$$\tau_{\text{res}} = \frac{t_{N_c}^{(c)}}{N_c} = 18.22 \text{ ps} \quad (4)$$

was obtained at room temperature. Moreover, once the bins were properly calibrated, the DNL was evaluated again, this time using calibrated times $t^{(c)}$ as

$$\text{DNL}_i^t = \begin{cases} 0 & \text{if } i=1, \\ \frac{t_i^{(c)} - t_{i-1}^{(c)} - \langle \Delta t^{(c)} \rangle}{\langle \Delta t^{(c)} \rangle} & \text{if } i > 1, \end{cases} \quad (5)$$

where $\langle \Delta t^{(c)} \rangle = \langle t_{i+1}^{(c)} - t_i^{(c)} \rangle = \tau_{\text{res}}$.

Lastly, to characterize the jitter of the system, a scheme like the one described in section II C was used, paired with a square wave as an input for both channels at room temperature. To obtain the jitter, a Gaussian fit was applied to the histogram of the difference between consecutive tags, from which the jitter was estimated as the $\text{FWHM} = 27.11 \text{ ps}$ (Fig. 5). We notice that the jitter is obtained by dividing by $\sqrt{2}$ the standard deviation of the Gaussian fit.

To determine the device performance with respect to environment changes, a temperature characterization of the system using the setup described in Section II C was performed. The data acquisition process consisted on storing, for each temperature, a file with the calibration curve for each channel along with the registered tags in non-calibrated format, with their respective channel. This format allowed to analyze the data with or without calibration, while also letting the possibility to implement calibration at particular points in the measurement. The acquired data for each temperature was processed in four different ways:

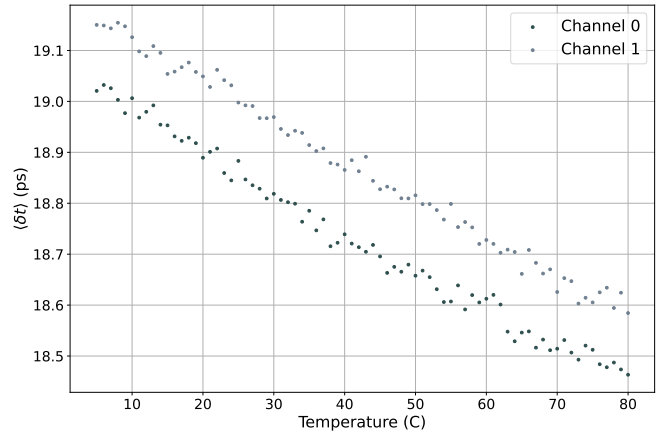


FIG. 6: Mean single-bin propagation time for each channel of the TDC as a function of the temperature of the chip. The different offset between both channels was attributed to non-uniformity of components in the chip.

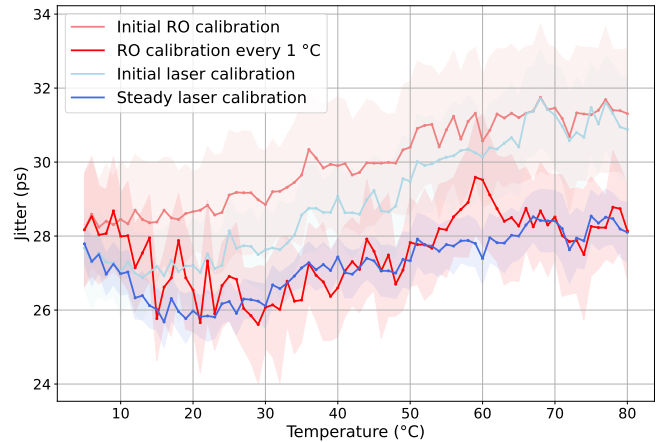


FIG. 7: Comparison of the jitter of the system as a function of temperature obtained for different calibration methods: with the RO at 5°C and maintained through the scan (light orange); with the RO every 1°C step (red); with the single photon detector at 5°C and maintained through the scan (light blue); and steadily with the single photon detector (blue).

1. Calibrated using the calibration curve obtained with the RO at 5°C (light orange curve in Fig. 7).
2. Calibrated using the first time tags registered with the single photon detector at 5°C (light blue curve in Fig. 7).
3. Calibrated using the calibration curve obtained for each temperature (red curve in Fig. 7).
4. Steadily calibrated (blue curve in Fig. 7).

As a first step, the relation between temperature and the average propagation time inside the delay line, $\langle \delta t \rangle$, was analysed. Since the maximum number of registered bins is temperature and channel dependent (obtaining around 130 bins for 5 °C and up to 136 for 80 °C), we restricted this analysis to the first 120 elements of the delay line, such that

$$\langle \delta t \rangle = \frac{\sum_{j=1}^{120} \delta t_j}{120}. \quad (6)$$

The observed behavior depends on the particular architecture and materials of the Zynq7020 chip (28 nm process), of which not much information is publicly available, concluding that the CARRY4 element has a propagation time that is, in average, inversely proportional to temperature.

Then, the jitter was calculated in the 4 scenarios previously mentioned (Fig. 7). For both cases in which the calibration was done just at 5 °C, increasing the chip temperature monotonically increased the jitter of the system (as also verified by *Alshehry et al.* in [26]), which highlights the importance of the steady calibration scheme, since the transistors' characteristics are temperature dependent. On the other hand, when applying a calibration for every temperature step, the jitter decreased until 30 °C, which implies an improvement in performance, and then increased until it stabilized at 60 °C, close to the starting value. Finally, the one obtained with the steady calibration had a very similar shape to the one obtained by calibrating at each temperature, but with two notable improvements. In first instance, the system's jitter was found to be more stable, presenting an average standard deviation $\langle \sigma_{\text{steady}} \rangle = 0.64$ ps, compared to the $\langle \sigma_{\text{RO}} \rangle = 1.33$ ps obtained for the case when RO calibration was performed before each measurement. Moreover, as previously mentioned, the steady calibration does not require the acquisition to be stopped at any time, thus allowing the system to not lose any data.

Finally, a test with a QKD polarization-encoded source and receiver scheme was performed. The width of the detected pulse depends on the width of the optical pulse itself, the jitter of the detector, and the jitter of the time tagger. For both devices, the mean QBER obtained was of 2.2 %⁴, showing that our design presents good performance for QKD applications. We compared the width of the detected pulse using both MARTY and the QuTAG, a high-level commercial time tagging system with 13.4 ps jitter on the standard version (Fig. 8). It was observed that, even though Marty's jitter was higher than the QuTAG, the pulse width obtained with both devices were comparable. This behaviour is due to most of the width of the pulse coming from the detector's jitter, which is considerable higher than the time-tagger (~ 100 ps). In-

deed, moving to a higher level FPGA technology (e.g., Ultrascale+ with 16 nm FinFET process) can considerably increase the device's performances [27].

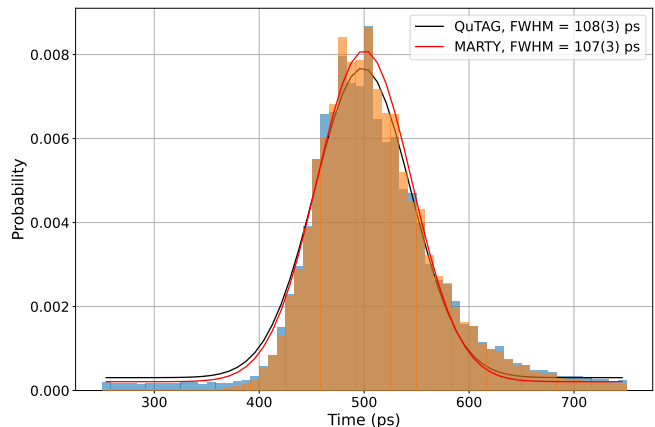


FIG. 8: Pulse shape obtained with MARTY (orange bars) and the QuTAG (blue bars), with their corresponding Gaussian fit.

IV. CONCLUSION

An FPGA-based time-to-digital converter, named MARTY, was implemented on a Zynq7020 FPGA, coupled with a unique calibration method which increases detection accuracy and removes data loss. This calibration method exploits single photon detection allowing it to calibrate the device at each new event and without stopping data acquisition. MARTY is capable of acquiring data continuously for up to one week of runtime before overflowing, with parameters compatible with state-of-the-art results, those being resolution $\tau_{\text{res}} = 18.22$ ps, DNL = $[-0.97, 2.86]$, and jitter $\tau_{\text{jitter}} = 27.11$ ps. The steady calibration method was tested between 5 °C and 80 °C, highlighting its validity as the jitter is kept under control while the temperature changing. Indeed, the steady calibration could be exploited in those environment that affect TDC performances becoming a key point of the dedicated application, like Satellite Quantum Communication. Moreover, MARTY was tested and compared with a high-level commercial TDC, using a QKD setup where the QBER obtained with both devices were equal, even with MARTY presenting a higher FWHM jitter. For future developments, an *online* version of the steady calibration feature could be implemented, while also upgrading to an Ultrascale+ (16 nm FinFET) based technology. This last point will increase the resolution and jitter even further thanks to a smaller process.

⁴ The QKD source and receivers were not properly optimized for

performance as it is outside the scope of this work.

- [1] S. Henzler, [Time-to-Digital Converters](#) (Springer Netherlands, Dordrecht, 2010).
- [2] S. Tancock, E. Arabul, and N. Dahnoun, A review of new time-to-digital conversion techniques, [IEEE Transactions on Instrumentation and Measurement](#) **68**, 3406 (2019).
- [3] A. Balla, M. Mario Beretta, P. Ciambone, M. Gatta, F. Gonnella, L. Iafolla, M. Mascolo, R. Messi, D. Moriciani, and D. Riondino, The characterization and application of a low resource fpga-based time to digital converter, [Nuclear Instruments and Methods in Physics Research Section A: Accelerators, Spectrometers, Detectors and Associated Equipment](#) **739**, 75 (2014).
- [4] C. Zhang, S. Lindner, I. M. Antolović, J. Mata Pavia, M. Wolf, and E. Charbon, A 30-frames/s, 252×144 spad flash lidar with 1728 dual-clock 48.8-ps tdc, and pixel-wise integrated histogramming, [IEEE Journal of Solid-State Circuits](#) **54**, 1137 (2019).
- [5] Q. Shen, S. Liao, S. Liu, J. Wang, W. Liu, C. Peng, and Q. An, An fpga-based tdc for free space quantum key distribution, [IEEE Transactions on Nuclear Science](#) **60**, 3570 (2013).
- [6] M. Avesani, L. Calderaro, M. Schiavon, A. Stanco, C. Agnesi, A. Santamato, M. Zahidy, A. Scriminich, G. Folletto, G. Contestabile, M. Chiesa, D. Rotta, M. Artiglia, A. Montanaro, M. Romagnoli, V. Sorianello, F. Vedovato, G. Vallone, and P. Villoresi, Full daylight quantum-key-distribution at 1550 nm enabled by integrated silicon photonics, [npj Quantum Information](#) **7**, 93 (2021).
- [7] S. Carrier, M. Labrecque-Dias, R. Tannous, P. Gendron, F. Nolet, N. Roy, T. Rossignol, F. Vachon, S. Parent, T. Jennewein, S. Charlebois, and J.-F. Pratte, Towards a multi-pixel photon-to-digital converter for time-bin quantum key distribution, [Sensors](#) **23**, 10.3390/s23073376 (2023).
- [8] A. Stanco, D. G. Marangon, G. Vallone, S. Burri, E. Charbon, and P. Villoresi, Efficient random number generation techniques for cmos single-photon avalanche diode array exploiting fast time tagging units, [Phys. Rev. Research](#) **2**, 023287 (2020).
- [9] J. Wang, S. Liu, Q. Shen, H. Li, and Q. An, A fully fledged tdc implemented in field-programmable gate arrays, [IEEE Transactions on Nuclear Science](#) **57**, 446 (2010).
- [10] B. Markovic, S. Tisa, F. A. Villa, A. Tosi, and F. Zappa, A high-linearity, 17 ps precision time-to-digital converter based on a single-stage vernier delay loop fine interpolation, [IEEE Transactions on Circuits and Systems I: Regular Papers](#) **60**, 557 (2013).
- [11] Y. Sano, Y. Horii, M. Ikeno, O. Sasaki, M. Tomoto, and T. Uchida, Subnanosecond time-to-digital converter implemented in a kintex-7 fpga, [Nuclear Instruments and Methods in Physics Research Section A: Accelerators, Spectrometers, Detectors and Associated Equipment](#) **874**, 50 (2017).
- [12] F. Garzetti, N. Corna, N. Lusardi, and A. Geraci, Time-to-digital converter ip-core for fpga at state of the art, [IEEE Access](#) **9**, 85515 (2021).
- [13] K. Hari Prasad and V. B. Chandratre, Calibration techniques in asic and fpga based time-to-digital converters, in [Topical Drifts in Intelligent Computing](#), edited by J. K. Mandal, P.-A. Hsiung, and R. Sankar Dhar (Springer Nature Singapore, Singapore, 2022) pp. 177–187.
- [14] S. Ito, S. Nishimura, H. Kobayashi, S. Uemori, Y. Tan, N. Takai, T. J. Yamaguchi, and K. Nitsui, Stochastic tdc architecture with self-calibration, in [2010 IEEE Asia Pacific Conference on Circuits and Systems](#) (2010) pp. 1027–1030.
- [15] Y.-H. Chen, Time resolution improvement using dual delay lines for field-programmable-gate-array-based time-to-digital converters with real-time calibration, [Applied Sciences](#) **9**, 10.3390/app9010020 (2019).
- [16] Y. Wang, W. Xie, H. Chen, and D. D.-U. Li, Multichannel time-to-digital converters with automatic calibration in xilinx zynq-7000 fpga devices, [IEEE Transactions on Industrial Electronics](#) **69**, 9634 (2022).
- [17] V. Scarani, H. Bechmann-Pasquinucci, N. J. Cerf, M. Dušek, N. Lütkenhaus, and M. Peev, The security of practical quantum key distribution, [Rev. Mod. Phys.](#) **81**, 1301 (2009).
- [18] L. Calderaro, A. Stanco, C. Agnesi, M. Avesani, D. Dequal, P. Villoresi, and G. Vallone, Fast and simple qubit-based synchronization for quantum key distribution, [Phys. Rev. Applied](#) **13**, 054041 (2020).
- [19] S. Pirandola, U. L. Andersen, L. Banchi, M. Berta, D. Bunandar, R. Colbeck, D. Englund, T. Gehring, C. Lupo, C. Ottaviani, J. L. Pereira, M. Razavi, J. Shamsul Shaari, M. Tomamichel, V. C. Usenko, G. Vallone, P. Villaresi, and P. Wallden, Advances in quantum cryptography, [Adv. Opt. Photonics](#) **12**, 1012 (2020).
- [20] W. Whitehead, Z. Nelson, K. Y. Camsari, and L. Theogarajan, Cmos-compatible ising and potts annealing using single-photon avalanche diodes, [Nature Electronics](#) **6**, 1009 (2023).
- [21] M. Adamič and A. Trost, A fast high-resolution time-to-digital converter implemented in a zynq 7010 soc, in [2019 Austrochip Workshop on Microelectronics \(Austrochip\)](#) (2019) pp. 29–34.
- [22] A. Stanco, F. B. L. Santagiustina, L. Calderaro, M. Avesani, T. Bertapelle, D. Dequal, G. Vallone, and P. Villoresi, Versatile and concurrent fpga-based architecture for practical quantum communication systems, [IEEE Transactions on Quantum Engineering](#) **3**, 1 (2022).
- [23] M. Mota and J. Christiansen, A high-resolution time interpolator based on a delay locked loop and an rc delay line, [IEEE Journal of Solid-State Circuits](#) **34**, 1360 (1999).
- [24] P. Carra, M. Bertazzoni, M. G. Bisogni, J. M. Cela Ruiz, A. Del Guerra, D. Gascon, S. Gomez, M. Morrocchi, G. Pazzi, D. Sanchez, I. Sarasola Martin, G. Sportelli, and N. Belcari, Auto-calibrating tdc for an soc-fpga data acquisition system, [IEEE Transactions on Radiation and Plasma Medical Sciences](#) **3**, 549 (2019).
- [25] F. Berra, C. Agnesi, A. Stanco, M. Avesani, S. Cocchi, P. Villoresi, and G. Vallone, Modular source for near-infrared quantum communication, [EPJ Quantum Technology](#) **10**, 27 (2023).
- [26] A. H. Alshehry, S. M. Alshahry, A. K. Alhazmi, and V. P. Chodavarapu, A study on the effect of temperature variations on fpga-based multi-channel time-to-digital converters, [Sensors](#) **23**, 10.3390/s23187672 (2023).

- [27] Y. Wang and C. Liu, A 3.9 ps time-interval rms precision time-to-digital converter using a dual-sampling method in an ultrascale fpga, [IEEE Transactions on Nuclear Science](#) **63**, 2617 (2016).

ACKNOWLEDGMENT

M.R.B.W. acknowledges support from the European Union's Horizon Europe Framework Programme under the Marie Skłodowska Curie Grant No. 101072637, Project Quantum-Safe Internet (QSI).

M.R.B.W. acknowledges funding from the italian gov-

ernment via a study scholarship granted by the Ministry of Foreign Affairs and International Cooperation (MAECI) A.Y. 2021-2022.

This work is (partially) supported by ICSC – Centro Nazionale di Ricerca in High Performance Computing, Big Data and Quantum Computing, funded by European Union – NextGenerationEU; Agenzia Spaziale Italiana, project Q-SecGroundSpace (Accordo n. 2018-14-HH.0, CUP: E16J16001490001); Agenzia Spaziale Italiana (2020-19- HH.0 CUP Grant No. F92F20000000005, Italian Quantum CyberSecurity I-QKD).

The authors would like to thank Dr. S. Bonora for the usage of the climatic chamber and Mr. A. Vanzo for the help in setting it up.